SUPPLEMENTARY INFORMATION

Methylation determines fibroblast activation and fibrogenesis in the kidney

Wibke Bechtel, Scott McGoohan, Elisabeth M. Zeisberg, Gerhard A. Müller, Hubert Kalbacher, David J. Salant, Claudia A. Müller, Raghu Kalluri and Michael Zeisberg

Contents:

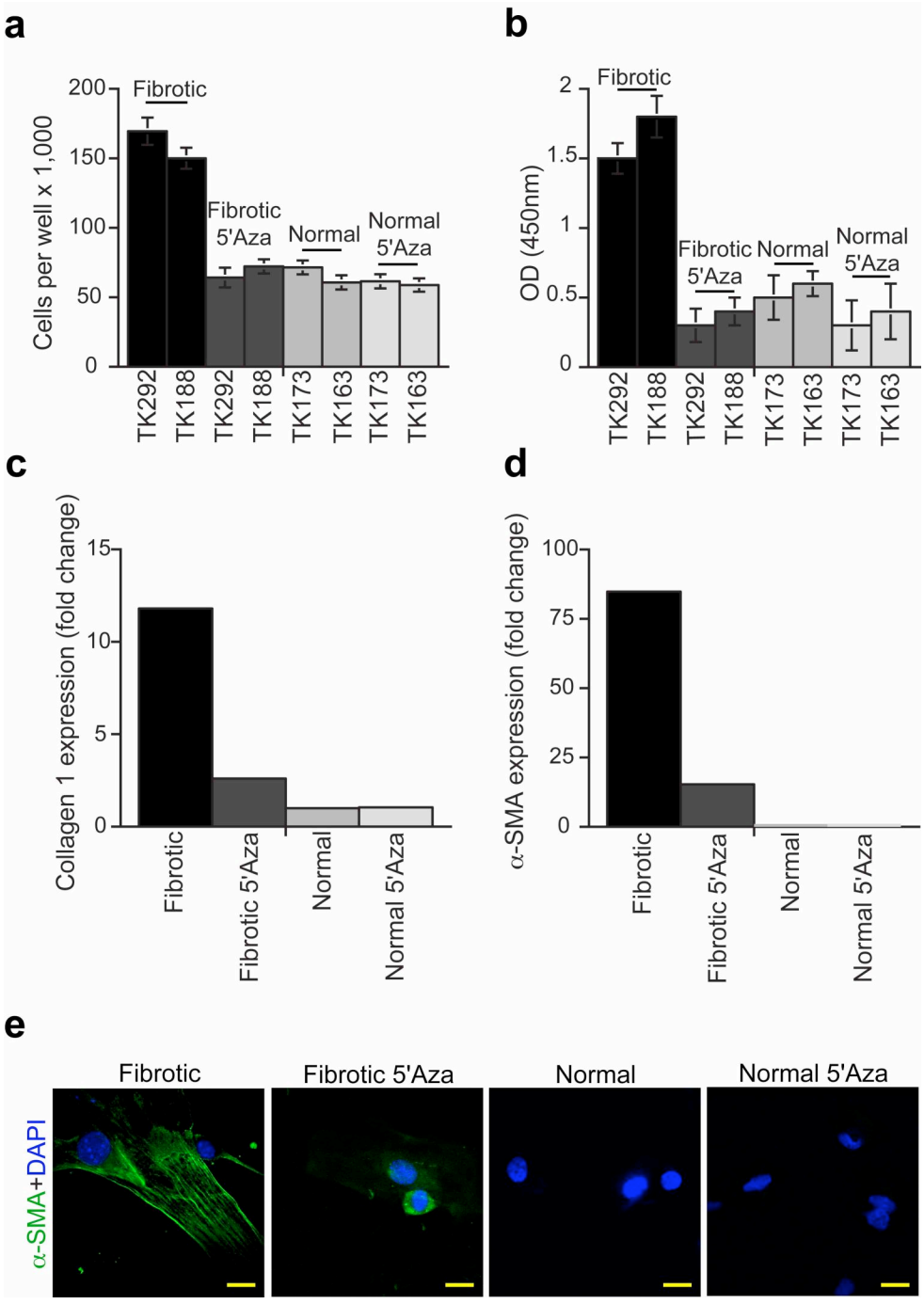

Supplementary Figure 1. 5'azacytidine normalizes fibrotic human kidney fibroblasts. **a.** Proliferation of primary human fibroblasts from fibrotic (TK292 and TK188) and non-fibrotic kidneys (TK173 and TK163) in response to 5'azacytidine. The graph summarizes average cell numbers after 96 hours. **b.** Type I collagen was analyzed

by ELISA in tissue culture supernatants of fibrotic and non-fibrotic kidney fibroblasts with or without 5'azacytidine incubation. The graph displays average relative OD readings of each group as assessed by quantitative real-time PCR. **c.** The bar graph summarizes relative expression levels of alpha2 chain of type I collagen of each group. **d.** Expression of α-SMA was quantified by real-time PCR. **e.** Fibroblasts were labeled with Fitc-conjugated antibodies to α-SMA (green). The pictures display representative photomicrographs of each group. Scale bars 20 μm.

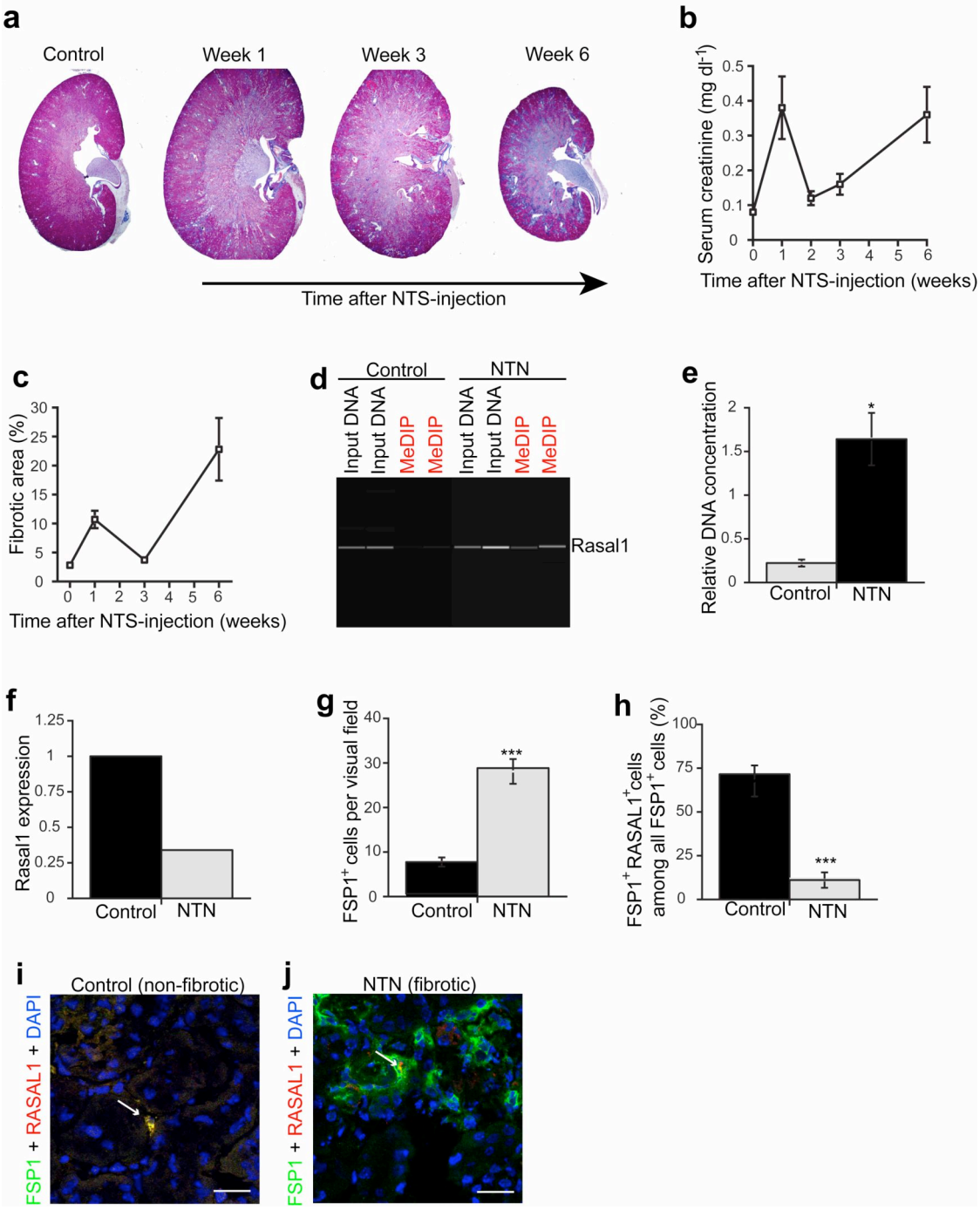

Supplementary Figure 2. *Rasal1* hypermethylation and transcriptional silencing in renal fibroblasts in the mouse model of nephrotoxic serum nephritis (NTN). a. The pictures display representative photomicrographs of Masson-Trichrome-stained kidney sections before, and one, three and six weeks after immunization with nephrotoxic

serum. Scale bars 200 μm. **b.** The graph summarizes average serum creatinine levels of mice before NTN injection (week 0), and at one, two, three and six weeks after NTN-injection. **c.** Average relative fibrotic area in kidneys of mice before NTN injection (week 0), and at one, three and six weeks after NTN-injection. **d.** The picture displays a virtual gel of methylated DNA immunoprecipitation analysis. PCR products of control input DNA and immunoprecipitated DNA (MeDIP) of non-fibrotic control kidneys and NTN kidneys (week 6) are displayed. **e.** The bar graph summarizes average DNA concentration of the methylated RASAL1 PCR product band in each group. The results were normalized to the corresponding input DNA. **f.** The graph summarizes RASAL1 expression levels in relation to control kidneys (week 0) during NTN progression. **g-j.** We performed immunofluorescence double-labeling experiments using antibodies to RASAL1 (red) and FSP1 (green). The graph in panel **g** summarizes the number of $FSP1^+$ fibroblast per visual field in each group. The graph in **h** summarizes average number of $FSP1^+RASAL1^+$ cells among all $FSP1^+$ fibroblasts per group. The picture in panel **i** displays a representative confocal photomicrograph of a non-fibrotic kidney, in panel **j** a confocal picture of a fibrotic kidney is displayed. $FSP1^+$ fibroblasts were predominantly $RASAL1^+$ in non-fibrotic kidneys (arrow). Scale bars 20 μm.* $P<0.05$; *** $P<0.001$.

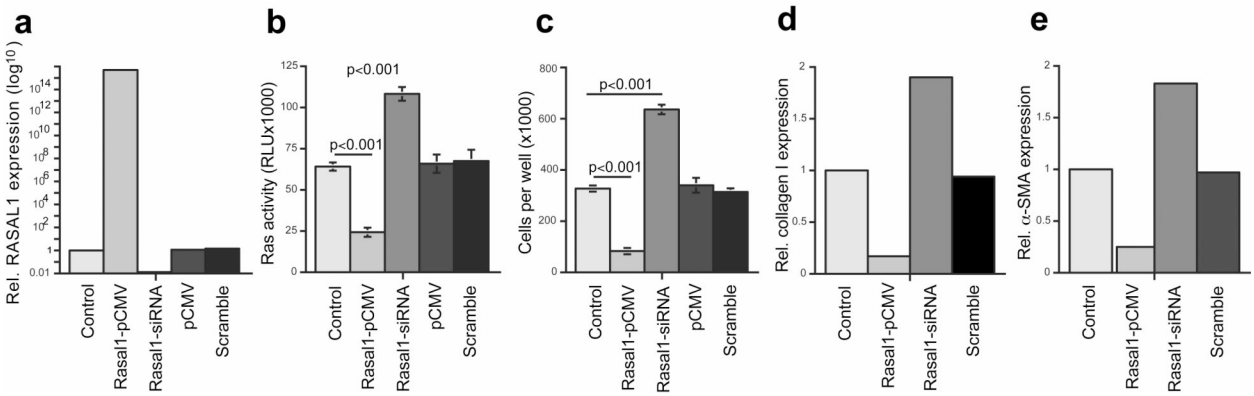

Supplementary Figure 3. RASAL1 expression determines renal fibroblast activation in human fibroblasts. a. 293 embryonic kidney fibroblasts were transfected with the pCMV6-XL-RASAL1 expression vector (RASAL1-pCMV) to increase RASAL1 expression levels, or with RASAL1 siRNA (RASAL1-siRNA) to decrease RASAL1. pCMV empty vector and scrambled siRNA were used as controls. The bar graph summarizes quantitative RT-PCR analysis of RASAL1 expression. **b.** The bar graph summarizes average Ras-GTPase activity in each group. **c.** 293 cells were seeded into 6-well plates at a density of 80,000 cells per well. The bar graph summarizes cell number of each group after three days in serum free media. **d.** Type I collagen expression by TK173 fibroblasts was assessed by quantitative real-time PCR using primers specific for the alpha2 chain of type I collagen. **e.** The bar graph summarizes average α-SMA expression in each group.

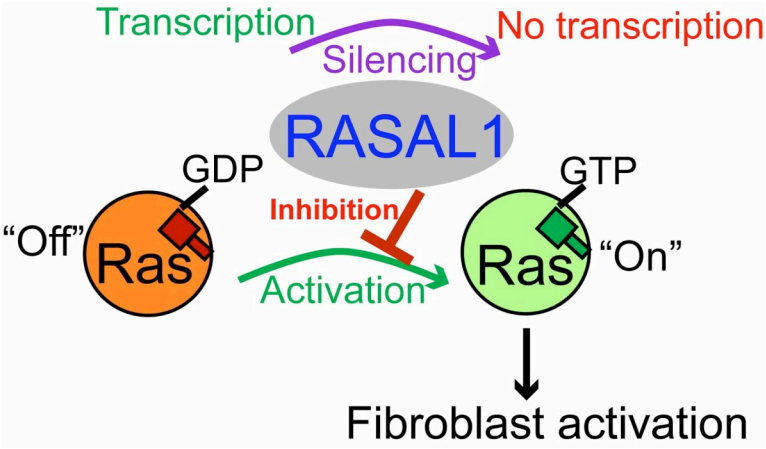

Supplementary Figure 4. RASAL1 silencing causes fibroblast activation. RASAL1 is a member of the RAS-GAP family, which catalyzes Ras inactivation by binding to GTP-Ras and catalyzing hydrolysis to GDP-Ras. Transcriptional silencing of RASAL1 causes Ras hyperactivity, ultimately leading to fibroblast activation.

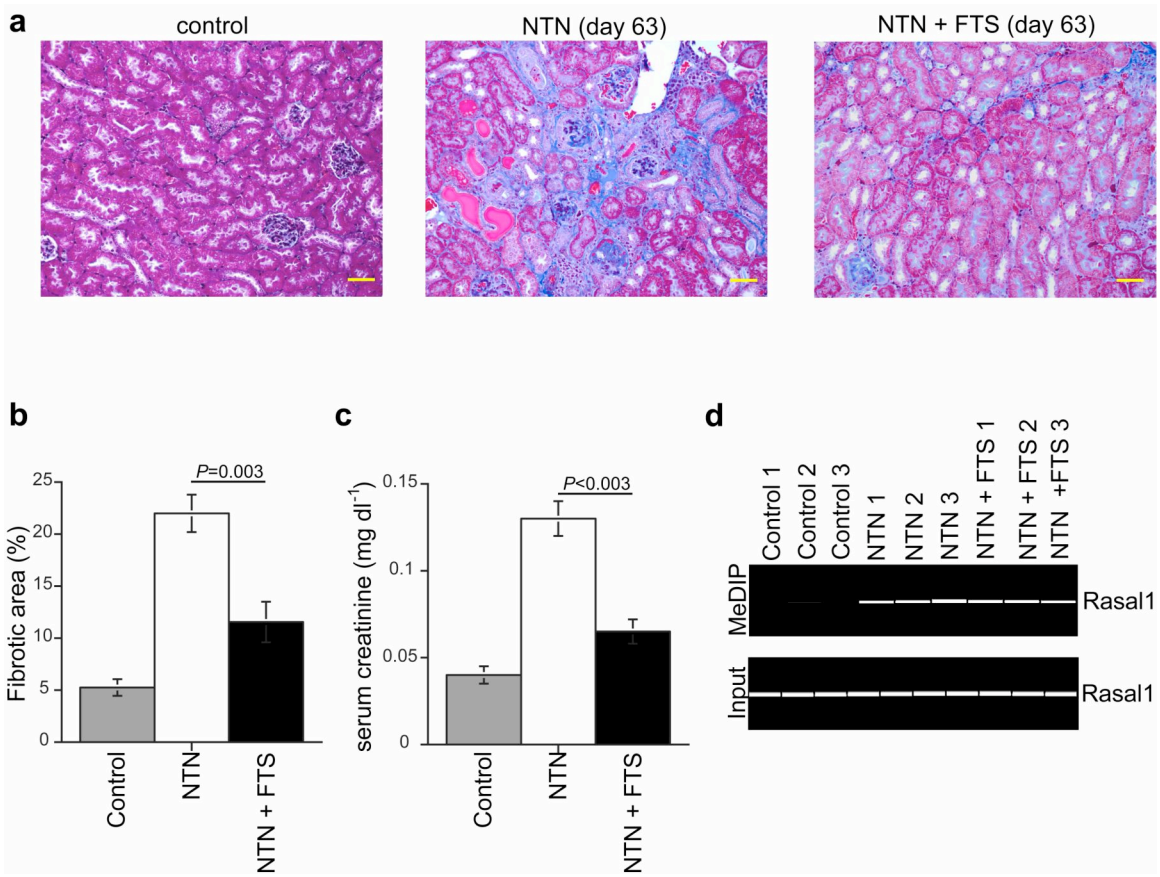

Supplementary Figure 5. Inhibition of Ras activity ameliorates renal fibrosis in the mouse model of nephrotoxic serum nephritis. a. The pictures display representative photomicrographs of MTS-stained kidneys of healthy C57BL/6 mice (control), of mice which had received nephrotoxic serum (9 weeks after immunization) and mice which had received treatment with the Ras-inhibitor FTS in addition to receiving nephrotoxic serum. Scale bars 20 μm. **b.** The bar graph summarizes the relative fibrotic area in each group. **c.** The bar graph summarizes average serum creatinine level (at day 63 after immunization). **d.** The picture displays representative virtual gels of *Rasal1* MeDIP analysis. The upper panel displays amplified methylated *Rasal1* DNA, the bottom picture displays the control input DNA.

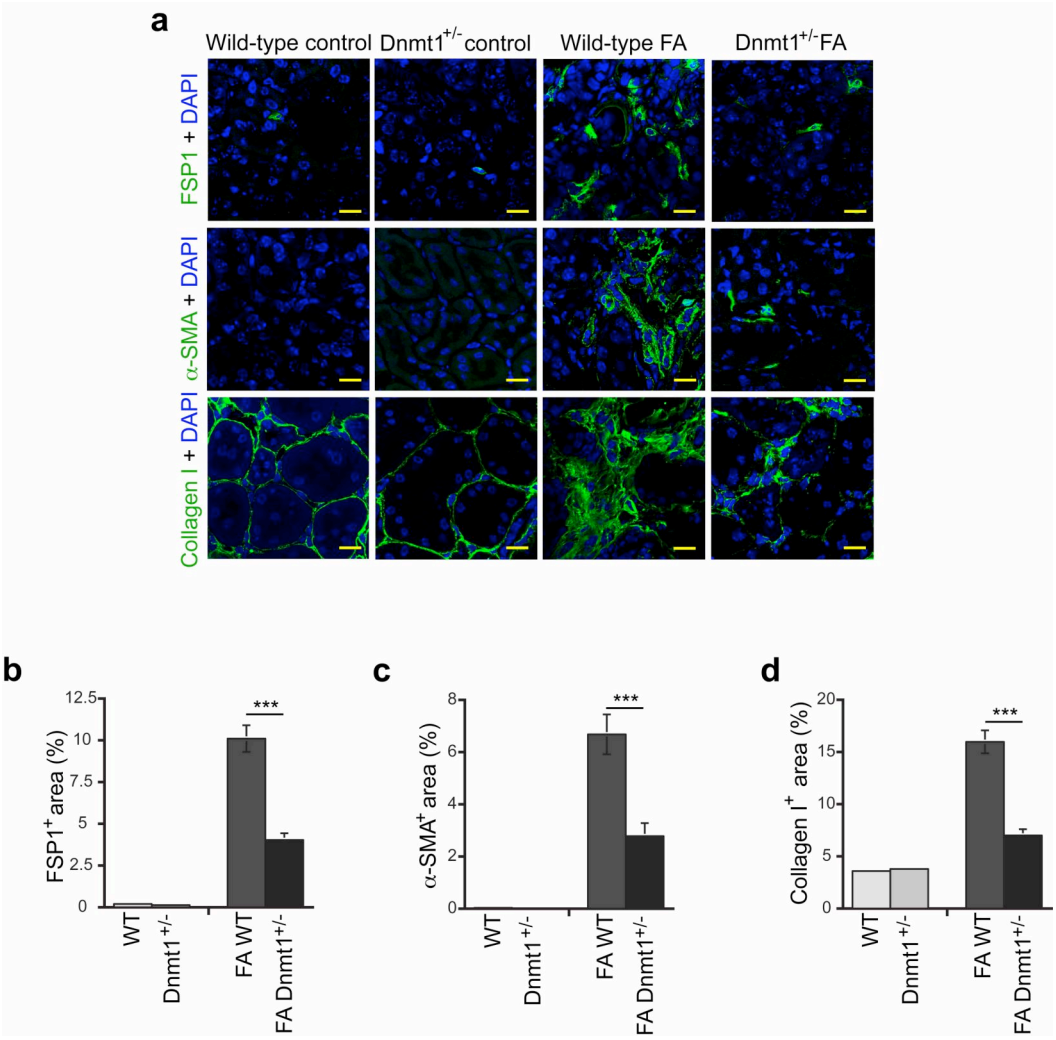

Supplementary Figure 6. Progression of Folic acid-induced nephropathy in *Dnmt1*$^{+/-}$ hemizygous deficient and wildtype mice. a. The pictures display representative confocal photomicrographs of C57BL/6 wildtype mice, of *DNMT*$^{+/-}$ mice, of C57BL/6 mice which had received folic acid 150 days prior to sacrifice and kidneys of *DNMT1*$^{+/-}$ mice which had been challenged with folic acid, all labeled with antibodies to FSP1 (top row), αSMA (middle row) and type I collagen (bottom row). Scale bars 20 μm. **b-d.** Staining analysis. The bar graphs summarize relative FSP1-labeled area **(b)**, relative αSMA-labeled area (**c**) and relative type I collagen-labeled area (**d**) in each group. *** P<0.01

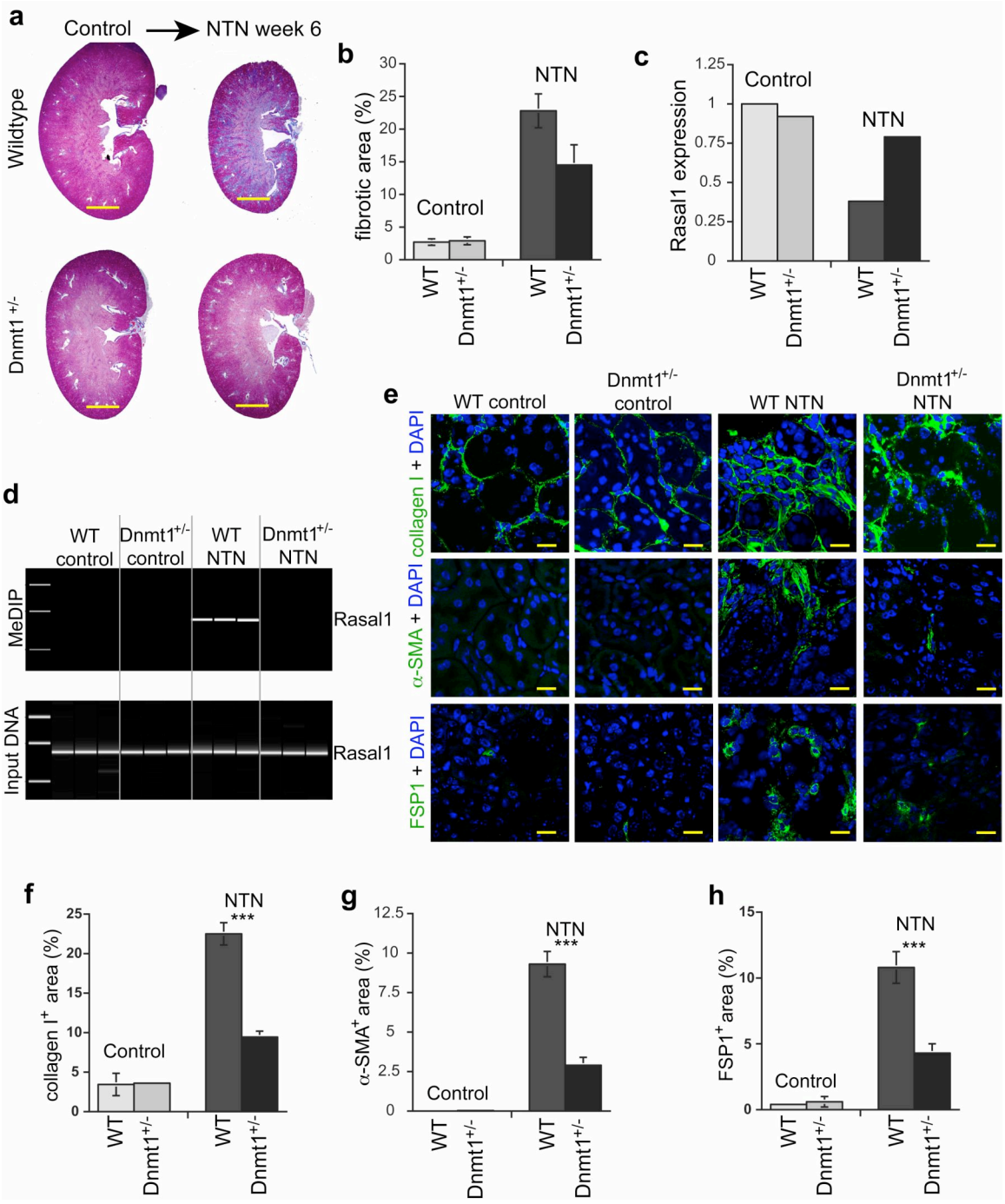

Supplementary Figure 7. Progression of Nephrotoxic serum nephritis (NTN) in *Dnmt1*$^{+/-}$ hemizygous deficient and wildtype mice. a. The panel displays MTS-stained kidney sections from wildtype and *Dnmt*$^{+/-}$ mice that were obtained before injection of NTN (left pictures) and six weeks after NTN-injection (right pictures). Scale bars 200 μm.

b. The graph summarizes average relative fibrotic area in kidneys of wildtype and *Dnmt1*$^{+/-}$ mice before NTN injection (control) and six weeks post NTN-injection. **c.** The graph summarizes Rasal1 expression levels in relation to wildtype control kidneys. **d.** **T**he picture displays a virtual gel of methylated DNA Immunoprecipitation analysis. PCR products of control input DNA (bottom panel) and immunoprecipitated *Rasal1* DNA (MeDIP, top panel) of wildtype NTN kidneys and NTN *Dnmt1*$^{+/-}$ kidneys (both six weeks after NTN injection) are displayed. **e.** Frozen kidney sections were labeled with antibodies to type I collagen (top row), αSMA (middle row) and FSP1 (bottom row). The pictures display representative confocal photomicrographs of each group. Scale bars 20 μm. **f-h.** The bar graphs summarize relative type I-collagen labeled area **(f)**, relative αSMA-labeled area (**g**) and relative FSP1-labeld area (**h**) in each group. *** $P<0.001$

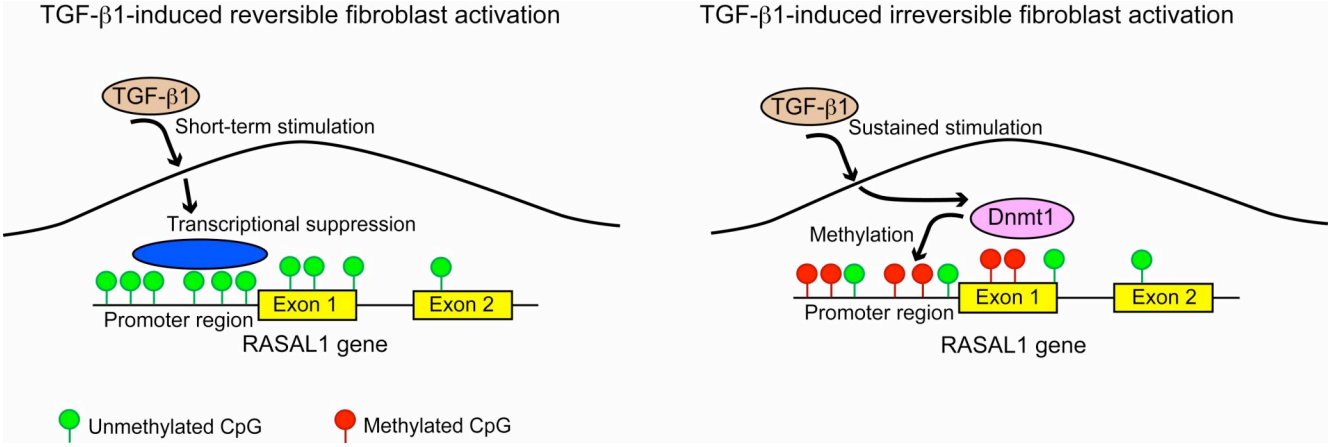

Supplementary Figure 8. Dual modes of RASAL1 silencing in TGFβ1-induced fibroblast activation. Our cell culture experiments suggest that TGFβ1 causes transcriptional silencing of *RASAL1* via two different mechanisms. **Left.** Short-term exposure of fibroblasts results in transcriptional suppression of *RASAL1* without hypermethylation. Such *RASAL1* suppression is reversible upon removal of TGFβ1. **Right.** Sustained exposure of fibroblasts (over 5 days) results in *RASAL1* hypermethylation. TGFβ1-induced *RASAL1* hypermethylation is dependent on the methyltransferase Dnmt1. Transcriptional suppression of *RASAL1* caused by hypermethylation is irreversible upon removal of TGFβ1.

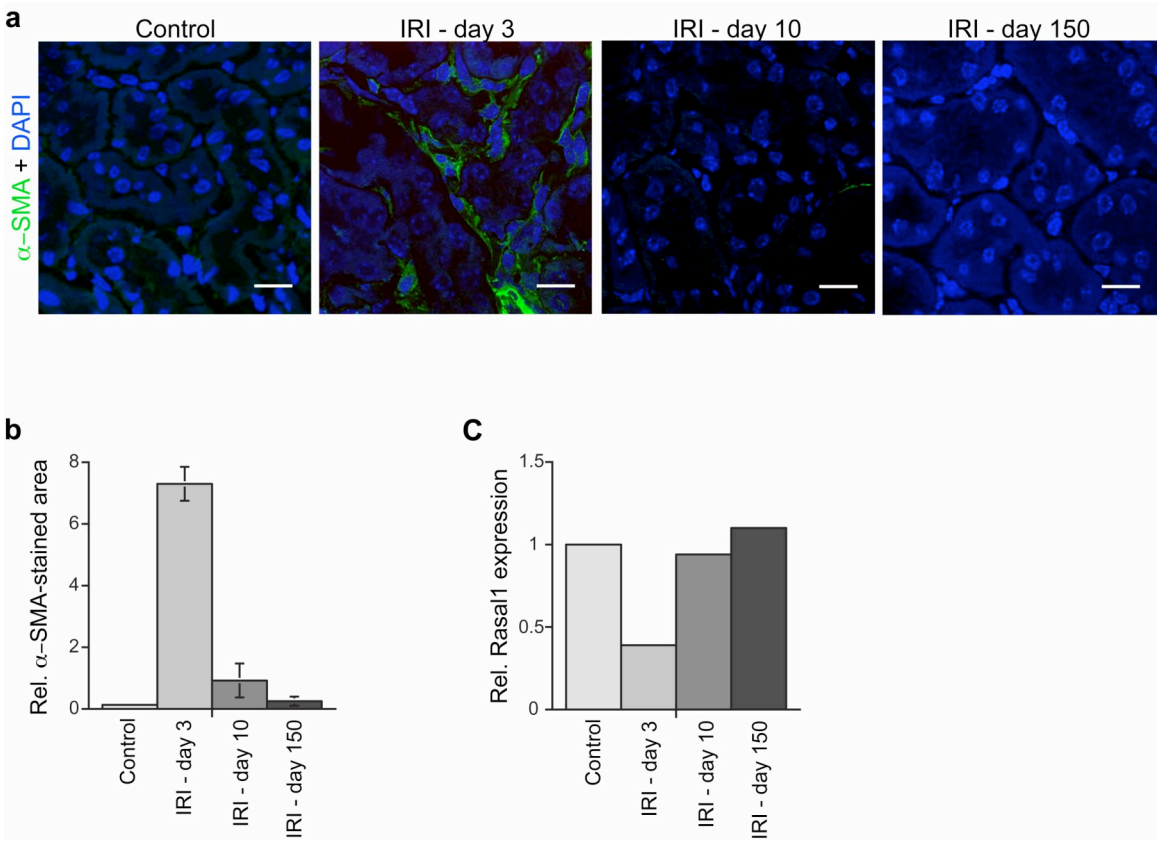

Supplementary Figure 9. Correlation of transient fibroblast activation and transient decrease of Rasal1 expression in reversible ischemia-reperfusion injury. **a.** The pictures display representative confocal photomicrographs of α-SMA -stained kidney sections from the indicated time-points after clamping of the renal pedicle for 30 minutes. Peak of injury three days after ischemia-reperfusion injury is associated with transient fibroblast accumulation. The kidney then spontaneously regenerates within 10 days associated with decrease of α-SMA$^+$ fibroblasts. Scale bars 20 μm. **b.** The bar graph summarizes relative αSMA-labeled area in each group. **c.** The graph summarizes Rasal1 expression levels in relation to control kidneys at each time-point.

Culture ID#	Histology	Fibrosis	Proli	αSMA	Col1	Array	MSP	BGS
TK 88	Mesangioproliferative GN	++	+	+	+		X	X
TK 110	Mesangioproliferative GN	+++	+	+	+	X	X	X
TK 124	Minimal Intercapillary GN	-	-	-	-		X	X
TK 150	Mesangioproliferative GN	++	+	+	+		X	X
TK 156	Severe Nephrosclerosis	+++	+	+	+	X	X	X
TK 163	Normal	-	-	-	-	X	X	X
TK 173	Minimal Change GN	-	-	-	-		X	X
TK 188	IgA Nephritis	+++	+	+	+		X	X
TK 210	Minimal Intercapillary GN	-	-	-	-	X	X	X
TK 213	Mesangioproliferative GN	+++	+	+	+		X	X
TK 239	Transplant Rejection	+++	+	+	+	X	X	X
TK 257	Endocapillary GN	+++	+	+	+	X	X	X
TK 260	Normal (RCC)	-	-	-	-	X	X	X
TK 261	Mesangioproliferative GN	++	+	+	+	X	X	X
TK 270	CAN	+++	+	+	+		X	X
TK 274	Wegener's Granulomatosis	+++	+	+	+	X	X	X
TK 282	Membranous GN	++	+	+	+	X	X	X
TK 284	Mesangioroliferative GN	+++	+	+	+		X	X
TK 292	IgA Nephritis	+++	+	+	+		X	X

Supplementary Table 1. *RASAL1* methylation in human renal fibroblasts.

Culture ID#. Primary kidney fibroblasts cultures were named in order of tissues received.
Histology. Summary of the pathological diagnoses of the biopsies of which the primary fibroblasts were derived. Normal kidney was intended for transplantation but could not be transplanted. Normal (RCC) was obtained from the unaffected part of kidneys that were removed due to renal cell carcinoma. CAN: Chronic allograft nephropathy.
Fibrosis. The biopsies were semiquantitatively scored by a pathologist for fibrosis (-: normal; +:mild fibrosis,: ++ robust fibrosis; +++: severe fibrosis).
Proli. + indicates increased proliferative activity of primary cultures.
αSMA. + indicates increased αSMA expression of primary cultures.
Col1. + indicates increased type I collagen synthesis by primary cultures.
Array. X indicates which fibroblast cultures were analyzed in genome-wide methylation screen.
MSP. X indicates which fibroblast cultures were analyzed by RASAL1 specific methylation specific PCR.
BGS. X indicates fibroblast cultures in which *RASAL1* methylation was analyzed by bisulfite genomic sequencing.

Name	Function	CpG in promoter in human and mouse	Decreased in fibrosis
DLG2	Function unknown (found in onkocytoma)	yes	no
Enc	Function unknown (eye development)	yes	no
Eya1	(kidney development)	yes	yes
Fez1/Lzts1	cell cycle inhibitor	no	no
HIPK1	Heat shock protein	yes	no
HIPK2	Heat shock protein	yes	no
HIPK3	Heat shock protein	yes	no
Lrfn2	neuronal transmembrane protein	yes	yes
Odd1	kidney development	yes	no
Pax3	kidney development	yes	no
RASAL1	Ras suppressor	yes	yes
Zu5	NF-kappaB inhibitor	no	no

Supplementary table 2: Methylated genes in fibrotic human renal fibroblasts.

Name. List of genes that were methylated in all tested fibrotic fibroblasts and in none of the non-fibrotic fibroblasts.

Function. Primary known function of the identified genes.

CpG in promoter in human and mouse. Presence of CpG islands within predicted promoter region in human and mice ("no" indicates not present in mouse).

Decreased in fibrosis. Decreased mRNA expression (at least two-fold) as determined by quantitative real-time PCR of total RNA lysates of fibrotic mouse kidneys.

Supplementary table 3

Real-time PCR primers

Primer	Name	Target sequence
hRASAL	hRASAL1-213F	CGTGCTGGATGAGGACACTG
	hRASAL1-275R	TCCCTGCTCAGCGAGATCTT
	hRASAL1-234T TaqMan® probe	FAM-CGGGCACGACGACATCATCGG-TAMRA
hαSMA	hαSMA -277F	GAAGAGCATCCCACCCTGC
	hαSMA -388R	ATTTTCTCCCGGTTGGCCT
	hαSMA -298T TaqMan® probe	FAM-ACGGAGGCACCCCTGAACCCC-TAMRA
hCol1A2	hCOL1A2-238F	GGTGAAGTGGGTCTTCCAGG
	hCOL1A2-307R	TAAGGCCGTTTGCTCCAGG
	hCOL1A2-259T TaqMan® probe	FAM-CTCTCCGGCCCCGTTGGACC-TAMRA
mCol1A1	mCol1A1-281F	ATGGATTCCCGTTCGAGTACG
	mCol1A1-343R	TCAGCTGGATAGCGACATCG
	mCol1A1-304T TaqMan® probe	FAM-AGCGAGGGCTCCGACCCCG-TAMRA
mRASAL1	mRasal1-316F	CTCACAAGGCGTGAGGTGG
	mRasal1-381R	TGCCAAGGAGTTAGAACGGAA
	mRasal1-336T TaqMan® probe	FAM-TCGAACCAATGACCCCAACACCCT-TAMRA
mαSMA	mαSMA -133F	CACTATTGGCAACGAGCGC
	mαSMA -192R	CCAATGAAGGAAGGCTGGAA
	mαSMA -153T TaqMan® probe	FAM-TCCGCTGCCCGGAGACCCT-TAMRA

siRNA Oligos

siRNA	Cat. No.	Target sequence
Mm_Rasal1_1	SI01397207 (Qiagen)	CTGGTGAAAGTGGATGACCAA
Mm_Rasal1_2	SI01397214 (Qiagen)	AACGTGAATGACCTCAACCAA
Mm_Rasal1_3	SI01397221 (Qiagen)	TGGGAAGATCTCATTGAGCAA
Mm_Rasal1_4	SI01397228 (Qiagen)	CACGCGCTTTGCCTTCAAGAA
Ctrl_AllStars_1	SI03650318 (Qiagen)	Proprietary of Qiagen, not disclosed
H_Rasal1_1	HSS112267 (Invitrogen)	UGGCUUUGCUGGAAGAGCUGACCUU
H_Rasal1_2	HSS112268 (Invitrogen)	GGGACCAGCUCAGGCUGAAAUUACU
H_Rasal1_3	HSS112269 (Invitrogen)	GGAUUCUAACAUGGAUACAACUCUG
Stealth™ siRNA	GC12935-300 (Invitrogen)	Proprietary of Qiagen, not disclosed

MeDIP primers

Primer	Target sequence
GADPH For	GTCGGTGTGAACGGATTTGGC
GADPH Rev	GCTCCTGGAAGATGGTGATGG
LAP For	TGCGACTTCCTGAGTATATGACCC
LAP Rev	GACCTTCAGTGGTTCTTCAGACAG
MethChIP For1	CTGGCTCAGCCTCCTGTTCTG
MethChIP Rev1	CAGACAACCCCGATCCAGGACC

MSP/BGS primers

Primer		Target sequence
Human RASAL1 MSP	RASALm11	GTGTATTTTTGTTTTCGTCGTTC
	RASALm2	CAAAGAACTCTTACCGAAACG
	RASALU3	AATTTATTAGGAGTTAGTGGTTAT
	RASALU2	CACAACAAACTCTTACCAAAACA
Human RASAL1 BGS1	RASALBGS1	GTTTAATGTTAATTTATTAGGAGTT
	RASALBGS3	CTAACCACAAACTTTCCAAACAA
Human RASAL1 BGS2	RASALBGS2_For	TAGTTTGTTTGTTTGGAGTTTTAGA
	RASALBGS2_Rev	ACCTACTTCAAACCTAACTCCCTAC

Cloning primers

hRASAL1RevCheckP	5'-CCAGGGTTAGATCCAGAACAG
hRASALMFP2 (XhoI)	5'-TACTCGAGATCACAGTGGGCCAGGCATGGTGGC
hRASALMRP1 (HindIII)	5'-TAAAGCTTCCGAAAGAGGAGAAGGTGTAGG